

Effects of thermal annealing and film thickness on the structural and optical properties of indium-tin-oxide thin films

Ding Xu¹, Wen Zhou^{1,*}, Yuxin Du¹, Junying Zhang¹, Wei Zhang^{1,*}, Jiangjing Wang^{1,*}

¹Center for Alloy Innovation and Design (CAID), State Key Laboratory for Mechanical Behavior of Materials, Xi'an Jiaotong University, Xi'an 710049, China.

E-mails: wen.zhou@xjtu.edu.cn, wzhang0@mail.xjtu.edu.cn, j.wang@xjtu.edu.cn

Abstract:

Indium-tin oxide (ITO) has been leveraged as a crucial functional layer in the optoelectronic frameworks, such as non-volatile color display thin films based on the ITO/phase-change material (PCM)/ITO/reflective metal multilayer structures on a silicon substrate. In addition to non-volatile color tuning by PCMs, phase transition of ITO may pose a substantial impact on display performances. Yet, a comprehensive colormap of ITO thin films as functions of annealing temperature and film thickness is missing. In this work, we systematically investigate properties of ITO films based on X-ray diffraction, spectroscopic ellipsometry and ultraviolet-visible spectrophotometry measurements. We provide a colormap of the ITO/platinum/silicon structure in terms of the annealing temperature (150–350°C) and thickness (5–100 nm) for the non-volatile color display, and we observe strong color changes under 250°C annealing treatment for the 50-nm and 100-nm-thick ITO films. We suggest that the intrinsic change in colors of the ITO functional thin-film layers should also be taken into account, when the PCM-based reconfigurable color devices are used in practice.

Introduction:

Indium-tin oxide (ITO) has been widely used as transparent conductive electrodes^[1-4] due to its excellent optoelectronic properties with mature deposition techniques^[5]. ITO shows a high transparency (>90%) in the visible spectrum^[6] with a high electrical conductivity^[7-8], making it as a crucial functional layer for the optoelectronic devices^[9-10], such as color display devices^[11-13]. Studies have been performed in the regulation of microstructures and properties of ITO thin films through annealing processes. In terms of microstructures, annealing treatment significantly enhances the crystallization properties of the ITO thin films, which introduce improvement in grain size, preferred orientation, and crystal integrity^[14-19]. It also leads to optimization of the surface morphology and reduction of roughness^[17-20]. Besides, annealing can effectively modulate the electrical properties of the ITO films, such as carrier concentration, mobility, resistivity, and their optical properties, including light transmittance, absorption, and optical band gaps^[6, 21-23], thereby optimizing the properties of ITO for optoelectronic platforms.

The ITO/phase-change material (PCM)/ITO/reflective metal multilayers on a silicon (Si) substrate^[11] acting as resonant optical cavities have been proposed for tunable color display^[24-27]. Figure 1a shows a schematic of the multilayer structure. The PCM can be $\text{Ge}_2\text{Sb}_2\text{Te}_5$ (GST), and the reflective metal layer can be platinum (Pt). This multilayer structure enables color switching and modulation through phase transition of the PCMs, offering an ultrafast color switching speed and a broad color gamut^[28]. The thickness of the top ITO layer ($t_{\text{ITO}1}$) is typically 5–20 nm. It serves as a capping layer to prevent GST from oxidation^[29-30]. In contrast, the thickness of the bottom ITO layer ($t_{\text{ITO}2}$) is thicker (50–150 nm) for regulating the base color^[11]. The structural phase transition of the GST layer from the amorphous to crystalline phases can be driven by thermal annealing on a hotplate or optical/electrical pulses induced annealing effect^[31-32]. Besides, melting and quenching processes based on a sequence of rapid heating and cooling by short pulses introduce a transition from crystalline to amorphous phases^[33-34]. Specifically, as shown in Figure 1b, crystallization of the GST is a multifold phase transition^[35-37], including amorphous to cubic phase transition under 150–220°C annealing and cubic to hexagonal phase transition under 260–350°C annealing through a vacancy ordering process^[38-43]. These transitions can produce significant changes in optical properties for tunable color display^[43-49].

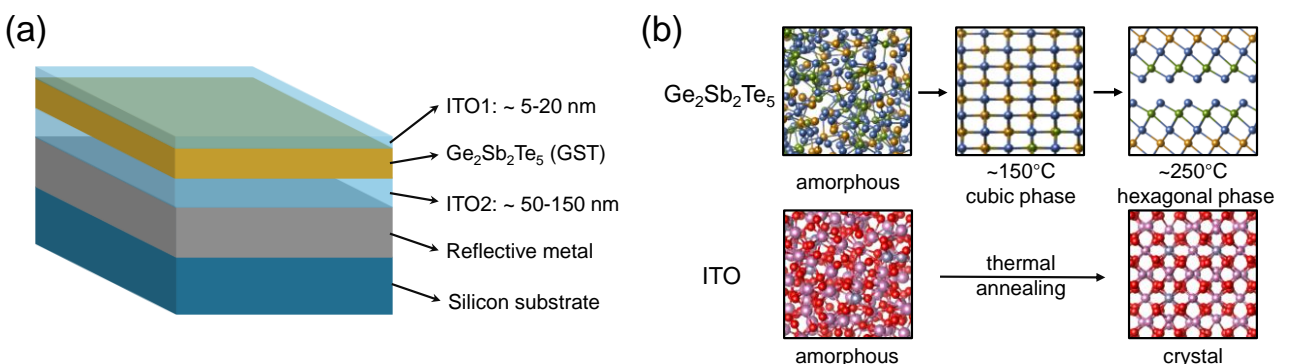


Figure 1. (a) Schematic of a reflective display multilayer thin-film structure consisting of ITO/GST/ITO/reflective metal layers on a silicon substrate. (b) Phase transition processes of GST and ITO by thermal annealing.

In addition to GST, CrTe_3 (~270°C)^[50-52], CrGeTe_3 (~270°C)^[53-55] and related two-dimensional layered

materials^[56-59], Ge-rich GST (above 350°C)^[60-62] and carbon-doped GST (330°C)^[63-66] all show high crystallization temperatures, which are even higher than that of ITO. For an example, crystallization temperatures have been characterized as ~250°C for the ITO thin film with a thickness of ~200 nm^[67]. Depending on the heating temperature and film thickness, the intrinsic properties of ITO can be changed significantly upon annealing^[68-72], leading to base color shifting of the multilayer structures. Crystallization of ITO affects the performance of color display, however, it has not been investigated in previous works^[11, 24-27]. A comprehensive colormap of ITO thin films as functions of annealing temperature and film thickness is missing.

Both crystallization of the PCM and ITO layers can contribute to the color changes of the ITO/PCM/ITO/Pt multilayer structures. To study the intrinsic properties of ITO, two basic structures, including ITO/Si and ITO/Pt/Si were used. We performed X-ray diffraction (XRD) and spectroscopic ellipsometry measurements of the ITO/Si structures versus ITO thickness and annealing temperature. A comprehensive refractive index data of ITO thin films has been established. While ITO exhibits a slower crystallization kinetics than those of PCMs, our characterizations demonstrate a strong modulation in refractive index upon crystallization. Finally, we established a comprehensive colormap of the ITO/Pt/Si structures as functions of film thickness (5–100 nm) and the annealing temperature (150–350°C). It shows obvious color changes under 250°C annealing treatment for the 50-nm and 100-nm-thick ITO thin films. Our quantitative experimental characterizations suggest that the intrinsic change in colors of the ITO thin-film layers should be taken into account in designing the PCM-based reconfigurable color devices.

Results

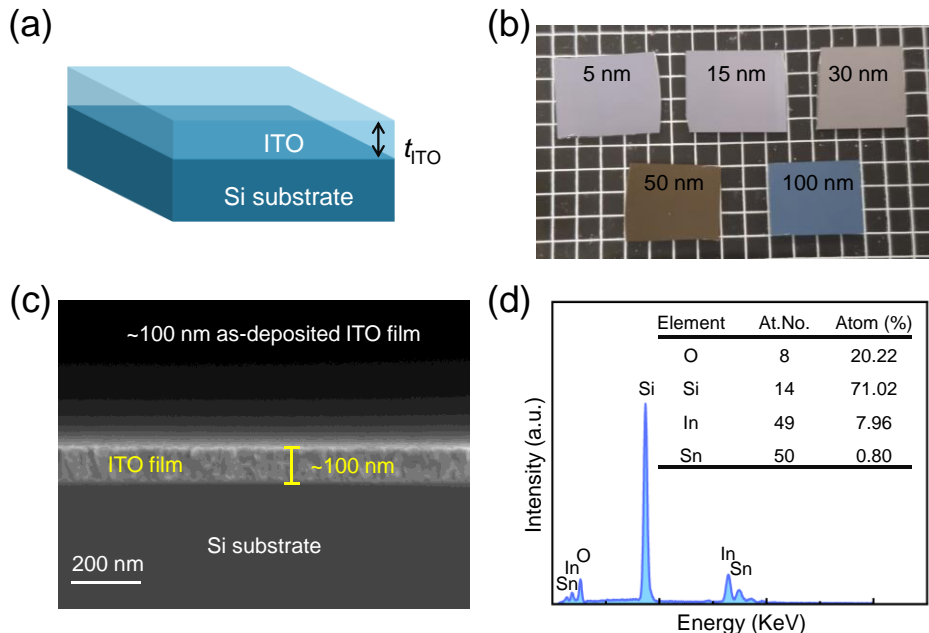


Figure 2. (a) Schematic of an ITO layer on a silicon (ITO/Si) substrate. (b) Photograph of ITO thin films deposited on Si substrates with varied ITO thickness (t_{ITO}). (c) A cross-sectional scanning electron microscopic (SEM) image of an ITO thin film deposited on a Si substrate. (d) Energy-dispersive X-ray spectroscopy (EDS) for an ITO thin film.

Figure 2a shows a schematic of an ITO thin film deposited on a silicon (ITO/Si) substrate with a film thickness of t_{ITO} . Figure 2b shows ITO thin films with different thicknesses (5 nm, 15 nm, 30 nm, 50 nm, and 100 nm) deposited on Si substrates using magnetron sputtering. Based on the optical interference effect, thickness variation introduces color changes of these ITO thin films. Figure 2c shows a cross-sectional scanning electron microscopic (SEM) image of the ITO sample, in which the thickness of ITO thin film was measured as ~ 100 nm. Figure 2d shows the energy-dispersive X-ray spectroscopy (EDS) measurement results for the ITO thin films. It shows characteristic peaks corresponding to indium (In), tin (Sn), Si, and oxygen (O) elements. Quantitative analysis reveals that the atomic percentage ratio of In:Sn is approximately 9.9:1, which matches well with the atomic ratio (9.8:1) of our ITO target (In_2O_3/SnO_2 90/10 wt%).

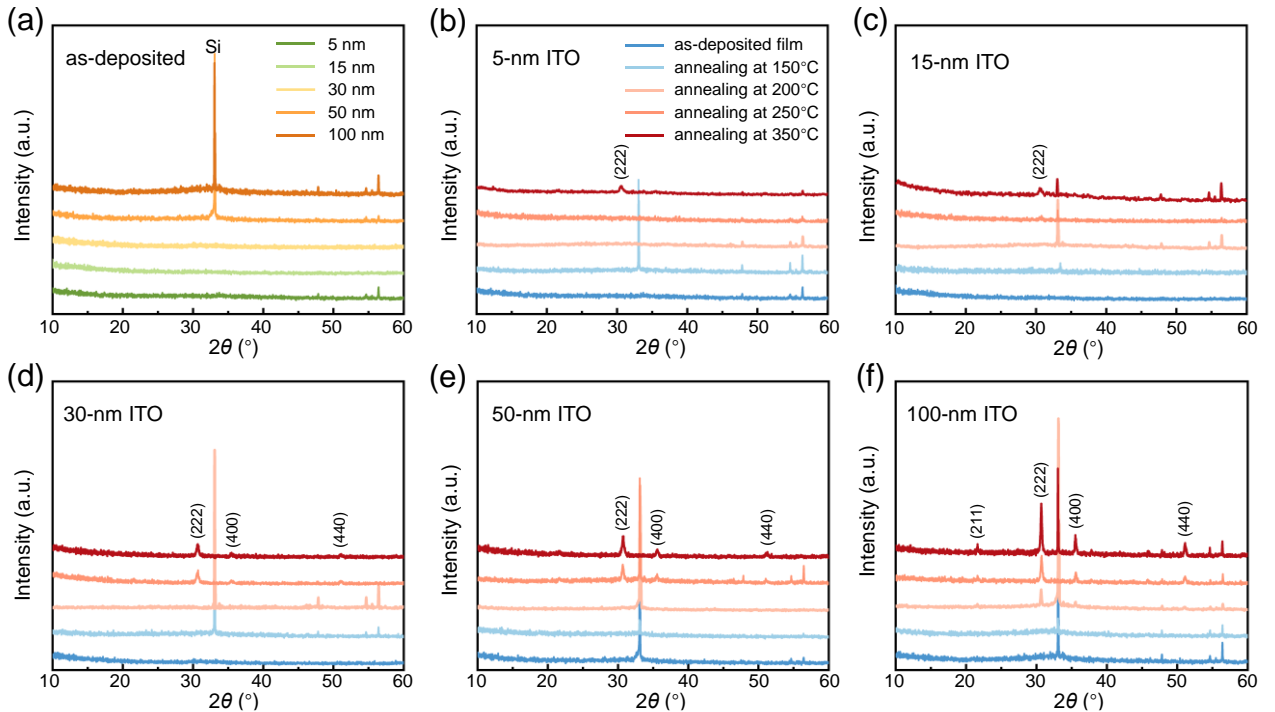


Figure 3. (a) X-ray diffraction (XRD) patterns of the as-deposited ITO samples with thicknesses of 5–100 nm. (b–f) XRD patterns of the as-deposited and annealed ITO samples with thicknesses of 5 nm (b), 15 nm (c), 30 nm (d), 50 nm (e), and 100 nm (f). These samples are annealed at temperatures of 150°C, 200°C, 250°C, and 350°C.

Figure 3 shows the XRD patterns of ITO samples with different thicknesses after annealing at temperatures of 150°C, 200°C, 250°C, 350°C. For all as-deposited ITO thin films, only the diffraction peaks of the Si substrate are observed as shown in Figure 3a, indicating the amorphous state of the ITO films. All films annealed at 150°C show no distinct characteristic peaks of ITO because the temperature is below the crystallization temperature of the amorphous ITO films^[73-74]. The (222) diffraction peak emerges for the 5-nm ITO film annealed at 350°C and 15-nm ITO film annealed at 250°C as shown in Figure 3b and Figure 3c, respectively. In addition to (222) peak, multiple diffraction peaks, such as (400) and (440), emerge for the 30-nm and 50-nm ITO films annealed at 250°C (Figure 3d and Figure 3e). The 100-nm ITO film (Figure 3f) shows a pronounced crystallization with diffraction peaks of (211), (222), (400), and (440) presented at 200°C. Thus, there is a strong correlation between the crystallization temperature and the film thickness. When the annealing temperature reaches 350°C, the 100-nm ITO sample shows a distinct XRD pattern with (211), (222),

(400), and (440) diffraction peaks, which can be assigned to the body-centered cubic structure of In_2O_3 (JCPDS Card No. 06-0416). Peaks corresponding to tin or tin oxides were not detected, indicating the absence of tin and its oxide clusters. All tin atoms are likely substitutionally doped into the In_2O_3 lattice.

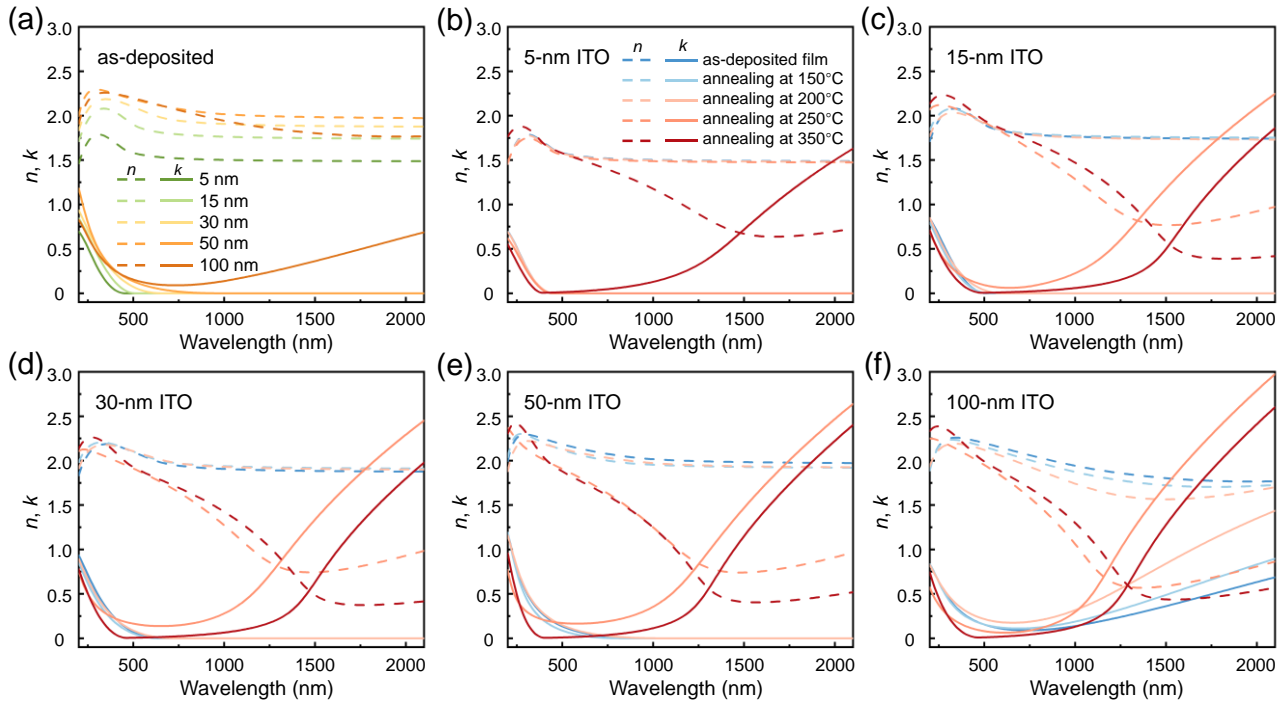


Figure 4. (a) Ellipsometry measurement of refractive indices of the as-deposited ITO samples with thicknesses of 5–100 nm. (b–f) Measured refractive indices of the as-deposited and annealed ITO samples with thicknesses of 5 nm (b), 15 nm (c), 30 nm (d), 50 nm (e), and 100 nm (f). These samples are annealed at temperatures of 150°C, 200°C, 250°C, and 350°C.

We next investigated the optical properties of the ITO films. ITO films with thickness of 5, 15, 30, 50 and 100 nm were sputtered onto Si substrates. The samples were characterized by spectroscopic ellipsometry. As shown in Figure 4, the optical constants of the thin films in a wavelength range of 200–2100 nm were extracted using the Drude-Lorentz model combined with a multilayer medium fitting algorithm. Figure 4a shows the measured optical constants (n , k) of the as-deposited ITO samples with thicknesses of 5–100 nm. In the visible light regime (400–760 nm), the refractive index (n) and extinction coefficient (k) of the as-deposited ITO films increase gradually with increase of ITO film thickness. This may be due to increase in carrier concentration of the amorphous film caused by the accumulation of oxygen vacancies or stress-induced changes in the electronic structure^[75–76]. Subsequently, the ITO films were annealed at various temperatures (150–350°C). Obvious changes in the optical constants occur upon crystallization of the ITO films as shown in Figure 4b–f, which are consistent with presence of the crystalline peaks in the XRD patterns as shown in Figure 3. The annealed and crystallized ITO films show decrease in refractive indices and increase in extinction coefficients^[77]. This can be explained by increase in the free carrier concentration after crystallization, which leads to enhancement in light absorption. Moreover, according to the Drude model describing the plasmonic behavior, increase in free electron density introduces a redshift in the plasma wavelength, which results in a decrease in the refractive index near the plasma edge^[78]. These results consistently demonstrate that the phase transition introduces obvious changes in the optical constants of ITO films.

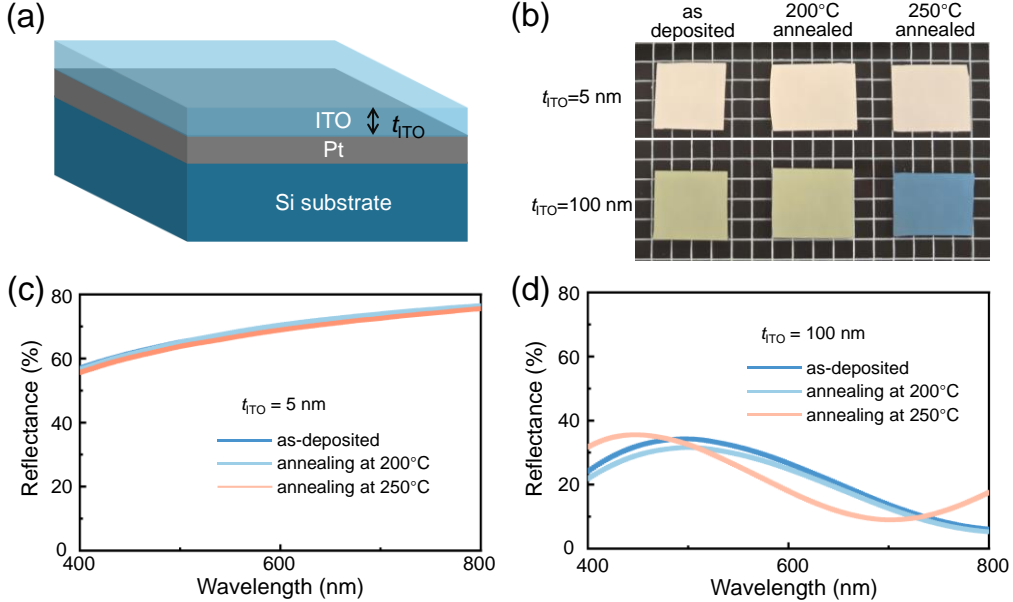


Figure 5. (a) Schematic of a reflective display thin-film structure consisting of an ITO layer and a Pt mirror coated on a Si substrate. (b) As-deposited and annealed samples with ITO thicknesses of 5 nm and 100 nm. (c) and (d) Reflection spectra of the as-deposited and annealed samples with ITO thicknesses of 5 nm (c) and 100 nm (d).

To investigate color regulation of ITO, we proposed a basic thin-film structure consisting of an ITO layer with a thickness of t_{ITO} and a Pt mirror deposited on a Si substrate (ITO/Pt/Si) with a schematic as shown in Figure 5a. These thin films can act as a resonant optical cavity, enabling tailorabile colors by adjusting the thickness or phase state of ITO. The ITO samples were further annealed at 200°C and 250°C to investigate tunable reflective colors. As shown in Figure 5b, when the thickness of ITO increases from 5 nm to 100 nm, the reflective color changes from light pink to yellow for the as-deposited ITO samples. The observed color changes in the samples clearly indicate that ITO thickness plays a crucial role. The colors of 5-nm and 100-nm-thick ITO samples show no notable change after thermal annealing at 200°C. However, a notable color change from yellow to blue was observed in the 100-nm-thick ITO sample annealed at 250°C. Figure 5c and Figure 5d show reflection spectra of the as-deposited and annealed samples with ITO thicknesses of 5 nm and 100 nm, respectively, measured by ultraviolet-visible spectrophotometry. For the 5-nm-thick ITO samples, it shows almost no variation in the reflection spectra after thermal annealing due to an ultrathin layer. However, there is an obvious blue shifting of the resonant peak wavelength from 500 nm to 450 nm by increasing annealing temperature from 200°C to 250°C for the 100-nm-thick ITO samples. This spectral blue shifting is consistent with the observed color evolution of the samples from yellow to blue.

To systematically examine color tunability of the ITO samples, we experimentally measured the reflection spectra of the samples versus ITO thickness and annealing temperatures by ultraviolet-visible spectrophotometry. We next converted the reflection spectra into the red-green-blue (RGB) colors to elaborate color display of these ITO thin films as shown in Figure 6a. It shows that the reflecting color can be tunable by increasing the ITO thickness or performing thermal annealing. As shown in Figure 6a, the chromaticity difference between the annealed and as-deposited ITO becomes more pronounced by increasing thickness. Notably, it shows obvious color variation under 250°C annealing treatment for the as-deposited ITO samples with thicknesses of 50 nm and 100 nm. We

further mapped the reflection spectra onto the CIE1931 chromaticity diagram by using the CIE color-matching equation^[79]. These achievable colors marked on the CIE1931 diagram are clearly separated except for those of the 5-nm-thick ITO samples as shown in Figure 6b. Among them, we can observe a relatively large color tuning range for the 50-nm-thick ITO samples. Thus, ITO/Pt/Si multilayer structures can be exploited for color display with obvious color changes when the ITO thickness is around or above 50 nm and annealing temperature above 250°C. Phase transition behavior of the ITO thin films may be useful for optical steganography and encryption applications^[80-81].

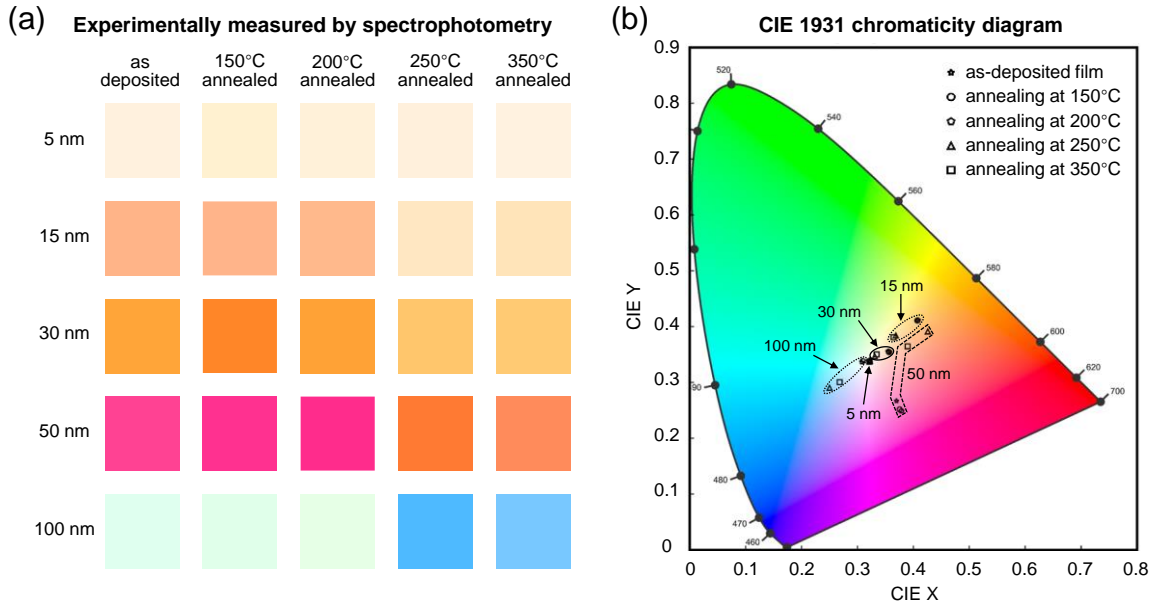


Figure 6. (a) Tunable reflecting color versus ITO thickness (5–100 nm) and thermal annealing temperature (150–350°C). (b) CIE1931 chromaticity diagram showing the achievable reflective colors of the as-deposited and annealed ITO samples versus thickness.

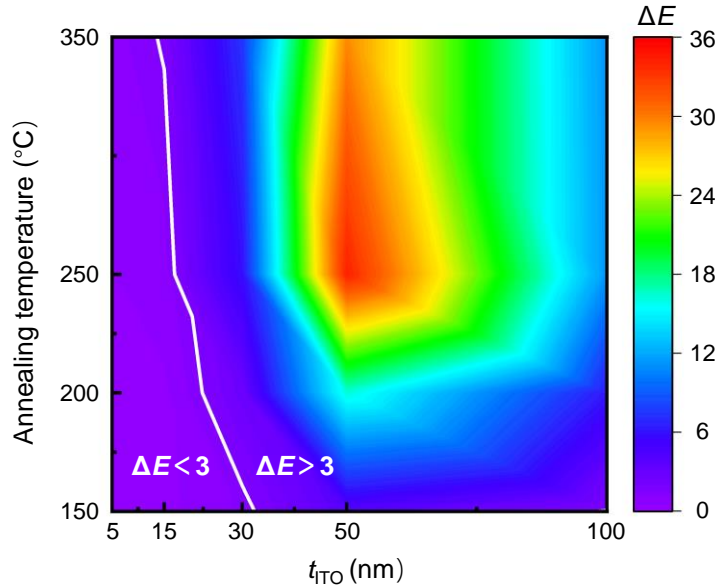


Figure 7. The contour of color difference (ΔE) versus ITO thickness and annealing temperature.

To quantitatively examine the color modulation performance, the color difference (ΔE) between the crystalline and as-deposited samples was calculated using the CIEDE2000 formula recommended by the International Commission on Illumination (CIE)^[82]. This formula provides superior visual perception agreement compared to the CIE76 standard^[81]. Figure 7 shows a calculated contour of ΔE versus ITO thickness and annealing temperature. Based on the human eye's threshold for color perception, we defined $\Delta E = 3$ as the evaluation criterion, and color changes are considered visually perceptible when ΔE exceeds this value. Under an annealing temperature of 250°C, ΔE reaches the maximum when ITO thickness is around 50 nm. By increasing annealing temperature, ΔE increases from 5.72 to 35.02 when the ITO thickness is fixed as 50 nm. In contrast, ITO layers impose a very weak effect in color modulation when the thickness is less than 15 nm, regardless of the thermal annealing temperature (150–350°C).

Summary

In summary, we systematically investigated effects of thermal annealing and film thickness on the structural and optical properties of ITO thin films for non-volatile color display. We performed XRD, ellipsometry, and ultraviolet-visible spectrophotometry measurements. Refractive indices of ITO thin films have been characterized as functions of thickness (5–100 nm) and annealing temperatures (150–350°C). Our measurements demonstrate a strong modulation in refractive index upon phase transition. We further exploited non-volatile color display application based on ITO thin film coated on a Pt mirror. We provided a comprehensive colormap of the ITO thin films in terms of film thickness and annealing temperature. By mapping the reflection spectra onto the CIE1931 chromaticity diagram, it shows strong color changes under 250°C annealing treatment for the 50-nm and 100-nm-thick ITO thin films. For the ITO/GST/ITO/Pt multilayer structures, annealing can be performed at 150–200°C to induce crystallization of the GST layer, in which ITO is most likely to persist in the amorphous phase with negligible impact on display performances according to our study on the colormap. However, thermally induced change in the intrinsic optical properties of ITO should be considered when annealing is performed for PCMs with high crystallization temperatures, such as CrTe₃^[50–52], CrGeTe₃^[53–55], Ge-rich GST^[60–62] and carbon-doped GST^[63–66]. If processing temperature is higher than the crystallization temperature of ITO during fabrication, ITO is most likely to be crystallized, and optical constants of the crystallized ITO should be used in the multilayer structure design. Therefore, our measured refractive index data of ITO as functions of annealing temperature and thickness is useful for developing PCM-based reconfigurable color devices.

Methods

Thin-film deposition: silicon wafers were ultrasonically cleaned in acetone, ethanol, and deionized water for 10 minutes each, and were dried with pure nitrogen gas. The ITO target (In₂O₃/SnO₂ 90/10 wt%) with a purity of 99.99% was adopted. ITO thin films were deposited on silicon wafers using the magnetron sputtering system (AJA Orion-8). Deposition process was carried out with a base pressure at $\sim 1 \times 10^{-7}$ Torr and an argon atmosphere at 3 mTorr. At room temperature, ITO thin films with thicknesses ranging from 5 nm to 100 nm were prepared by adjusting the deposition time with a direct current (DC) power of 60 W. The platinum metal mirrors were fabricated by depositing a 5-nm-thick chromium adhesion layer and a 100-nm-thick platinum layer via DC sputtering at 50 W power onto a silicon substrate.

Material characterization: thickness and composition of the thin-film samples were characterized using a scanning electron microscope (SEM; Sigma 300, Zeiss) with build-in energy-dispersive spectroscopy (EDS; XFlash 7, Bruker). X-ray diffraction (XRD) measurements were performed using a Bruker D8 ADVANCE diffractometer with Cu-K α radiation ($\lambda = 1.54056$ Å) over a 2θ range of 10° – 60° and a scanning step of 0.02° . Spectroscopic ellipsometry measurements were performed using a rotating compensator ellipsometer (UVISEL PLUS, Horiba) at a 70° incidence angle. The optical constants including refractive index and extinction coefficient were extracted by fitting the experimental data with the CODE™ software (<https://wtheiss.com>). Reflectance spectra were measured via UV-Vis-NIR spectrophotometry (Lambda 950, PerkinElmer) with a 2-nm step resolution across a wavelength range of 400–800 nm.

Acknowledgments

The work is supported by 111 Project (B25007). The authors acknowledge the Instrumental Analysis Center of Xi'an Jiaotong University.

Conflict of interest

The authors declare no conflict of interest.

Author Contributions

Ding Xu: data curation (lead); formal analysis (lead); investigation (lead); writing—original draft (equal). **Wen Zhou**: conceptualization (equal); data curation (equal); investigation (equal); writing—original draft (equal). **Yuxin Du**: data curation (equal); investigation (equal). **Junying Zhang**: data curation (equal); investigation (equal). **Wei Zhang**: conceptualization (lead); funding acquisition (lead); supervision (lead); writing—review and editing (lead). **Jiangjing Wang**: conceptualization (equal); supervision (equal); writing—review and editing (equal).

Data Availability Statement

The data that support the findings of this study are available from the corresponding author upon reasonable request.

References

- [1] T. Minami, *Semicond. Sci. Technol.* 2005, **20**, S35.
- [2] M. Katayama, *Thin Solid Films* 1999, **341**, 140.
- [3] U. Betz, M. Kharrazi Olsson, J. Marthy, M. F. Escolá, F. Atamny, *Surf. Coat. Technol.* 2006, **200**, 5751.
- [4] C. Guillén, J. Herrero, *Thin Solid Films* 2011, **520**, 1.
- [5] K. Ellmer, *Nat. Photon.* 2012, **6**, 809.
- [6] J. Zhang, X. Li, M. Zhong, Z. Zhang, M. Jia, J. Li, X. Gao, L. Chen, Q. Li, W. Zhang, D. Xu, *Small* 2022, **18**, 2201716.
- [7] V. Teixeira, H. N. Cui, L. J. Meng, E. Fortunato, R. Martins, *Thin Solid Films* 2002, **420**, 70.
- [8] C. Yuan, X. Liu, C. Ge, W. Li, K. Li, L. Fu, X. Zeng, H. Song, Y. He, X. Xiao, J. Gong, C. Chen, J. Tang, *ACS Appl. Mater. Interfaces* 2022, **14**, 49937.
- [9] Y. Han, Z. Hu, W. Zha, X. Chen, L. Yin, J. Guo, Z. Li, Q. Luo, W. Su, C. Q. Ma, *Adv. Mater.* 2022, **34**, 2110276.
- [10] J. Lee, H. Jung, J. Lee, D. Lim, K. Yang, J. Yi, W.-C. Song, *Thin Solid Films* 2008, **516**, 1634.
- [11] P. Hosseini, C. D. Wright, H. Bhaskaran, *Nature* 2014, **511**, 206.
- [12] J.-L. Wang, Y.-R. Lu, H.-H. Li, J.-W. Liu, S.-H. Yu, *J. Am. Chem. Soc.* 2017, **139**, 9921.

[13] F. I. Wu, X. H. Yang, D. Neher, R. Dodd, Y. H. Tseng, C. F. Shu, *Adv. Funct. Mater.* 2007, **17**, 1085.

[14] H. R. Fallah, M. Ghasemi, A. Hassanzadeh, H. Steki, *Mater. Res. Bull.* 2007, **42**, 487.

[15] Z. Fang, J. Zheng, A. Saxena, J. Whitehead, Y. Chen, A. Majumdar, *Adv. Opt. Mater.* 2021, **9**, 2002049.

[16] Z. Xu, P. Chen, Z. Wu, F. Xu, G. Yang, B. Liu, C. Tan, Z. Xu, L. Zhang, R. Zhang, Y. Zheng, *J. Mater. Sci. Mater. Electron.* 2014, **25**, 2287.

[17] M. Gulen, G. Yildirim, S. Bal, A. Varilci, I. Belenli, M. Oz, *J. Mater. Sci. Mater. Electron.* 2012, **24**, 467.

[18] S. D. Senol, A. Senol, O. Ozturk, M. Erdem, *J. Mater. Sci. Mater. Electron.* 2014, **25**, 4992.

[19] D. Ali, M. Z. Butt, I. Muneer, F. Bashir, M. Saleem, *Optik* 2017, **128**, 235.

[20] J. Xu, Z. Yang, H. Wang, H. Xu, X. Zhang, *Mater. Sci. Semicond. Process.* 2014, **21**, 104.

[21] H. Morikawa, M. Fujita, *Thin Solid Films* 2000, **359**, 61.

[22] Y. Chao, W. Tang, X. Wang, *J. Mater. Sci. Technol.* 2012, **28**, 325.

[23] M. Ahmed, A. Bakry, A. Qasem, H. Dalir, *Opt. Mater.* 2021, **113**, 110866.

[24] C. Ríos, P. Hosseini, R. A. Taylor, H. Bhaskaran, *Adv. Mater.* 2016, **28**, 4720.

[25] X. Chen, Y. Xue, Y. Sun, J. Shen, S. Song, M. Zhu, Z. Song, Z. Cheng, P. Zhou, *Adv. Mater.* 2022, **35**, 2203909.

[26] Z. Cheng, T. Milne, P. Salter, S. J. Kim, S. Humphrey, M. Booth, H. Bhaskaran, *Sci. Adv.* 2021, **7**, eabd7097.

[27] S. Tao, Q. Li, J. Wang, X. Wang, J. Cai, S. Li, W. Xu, K. Zhang, C. Hu, *Adv. Opt. Mater.* 2020, **8**, 2000062.

[28] Y. Lyu, S. Mou, Z. Ni, Y. Bai, Y. Sun, Z. Cheng, *Opt. Express* 2017, **25**, 1405.

[29] L. Wang, J. Wen, C. Yang, B. Xiong, *Sci. Technol. Adv. Mater.* 2018, **19**, 791.

[30] J. W. Seo, J.-W. Park, K. S. Lim, J.-H. Yang, S. J. Kang, *Appl. Phys. Lett.* 2008, **93**, 223505.

[31] K. Kato, M. Kuwahara, H. Kawashima, T. Tsuruoka, H. Tsuda, *Appl. Phys. Express* 2017, **10**, 072201.

[32] Y. Qu, Q. Li, L. Cai, M. Pan, P. Ghosh, K. Du, M. Qiu, *Light: Sci. Appl.* 2018, **7**, 26.

[33] K. Shportko, S. Kremers, M. Woda, D. Lencer, J. Robertson, M. Wuttig, *Nat. Mater.* 2008, **7**, 653.

[34] H. Taghinejad, S. Abdollahramezani, A. A. Eftekhari, T. Fan, A. H. Hosseini, O. Hemmatyar, A. Eshaghian Dorche, A. Gallmon, A. Adibi, *Opt. Express* 2021, **29**, 20449.

[35] T.-T. Jiang, X.-D. Wang, J.-J. Wang, H.-Y. Zhang, L. Lu, C. Jia, M. Wuttig, R. Mazzarello, W. Zhang, E. Ma, *Fundam. Res.* 2024, **4**, 1235.

[36] N. Bala, B. Khan, K. Singh, P. Singh, A. P. Singh, A. Thakur, *Mater. Adv.* 2023, **4**, 747.

[37] I. Ronneberger, W. Zhang, H. Eshet, R. Mazzarello, *Adv. Funct. Mater.* 2015, **25**, 6407.

[38] W. Zhang, R. Mazzarello, M. Wuttig, E. Ma, *Nat. Rev. Mater.* 2019, **4**, 150.

[39] X. Chen, S. Zhang, K. Liu, H. Li, Y. Xu, J. Chen, Y. Lu, Q. Wang, X. Feng, K. Wang, Z. Liu, T. Cao, Z. Tian, *ACS Photon.* 2022, **9**, 1638.

[40] Y. Zheng, Y. Wang, T. Xin, Y. Cheng, R. Huang, P. Liu, M. Luo, Z. Zhang, S. Lv, Z. Song, S. Feng, *Commun. Chem.* 2019, **2**, 13.

[41] Y. Zhou, W. Zhang, E. Ma, V. L. Deringer, *Nat. Electron.* 2023, **6**, 746.

[42] M. Wuttig, N. Yamada, *Nat. Mater.* 2007, **6**, 824.

[43] A. V. Kolobov, P. Fons, A. I. Frenkel, A. L. Ankudinov, J. Tominaga, T. Uruga, *Nat. Mater.* 2004, **3**, 703.

[44] Z. Xu, C. Chen, Z. Wang, K. Wu, H. Chong, H. Ye, *RSC Adv.* 2018, **8**, 21040.

[45] G. Bakan, S. Ayas, T. Saidzoda, K. Celebi, A. Dana, *Appl. Phys. Lett.* 2016, **109**, 071109.

[46] C. Ruiz de Galarreta, S. G. C. Carrillo, Y. Y. Au, E. Gemo, L. Trimby, J. Shields, E. Humphreys, J. Faneca, L. Cai, A. Baldycheva, J. Bertolotti, C. D. Wright, *J. Opt.* 2020, **22**, 114001.

[47] Q. He, N. Youngblood, Z. Cheng, X. Miao, H. Bhaskaran, *Opt. Express* 2020, **28**, 39841.

[48] M. Wuttig, H. Bhaskaran, T. Taubner, *Nat. Photon.* 2017, **11**, 465.

[49] Q. Wang, E. T. F. Rogers, B. Gholipour, C.-M. Wang, G. Yuan, J. Teng, N. I. Zheludev, *Nat. Photon.* 2015, **10**, 60.

[50] X. Wang, R. Wang, S. Sun, D. Xu, C. Nie, Z. Zhou, C. Wen, J. Zhang, R. Chu, X. Shen, W. Zhou, Z. Song, J.-J. Wang,

E. Ma, W. Zhang, *Nat. Mater.* 2025, 1.

[51] M. A. McGuire, V. O. Garlea, S. Kc, V. R. Cooper, J. Yan, H. Cao, B. C. Sales, *Phys. Rev. B* 2017, **95**, 144421.

[52] R. Li, J.-H. Nie, J.-J. Xian, J.-W. Zhou, Y. Lu, M.-P. Miao, W.-H. Zhang, Y.-S. Fu, *ACS Nano* 2022, **16**, 4348.

[53] C. Gong, L. Li, Z. Li, H. Ji, A. Stern, Y. Xia, T. Cao, W. Bao, C. Wang, Y. Wang, Z. Q. Qiu, R. J. Cava, S. G. Louie, J. Xia, X. Zhang, *Nature* 2017, **546**, 265.

[54] S. Hatayama, Y. Sutou, S. Shindo, Y. Saito, Y.-H. Song, D. Ando, J. Koike, *ACS Appl. Mater. Interfaces* 2018, **10**, 2725.

[55] X. Wang, S. Sun, J. J. Wang, S. Li, J. Zhou, O. Aktas, M. Xu, V. L. Deringer, R. Mazzarello, E. Ma, W. Zhang, *Adv. Sci.* 2023, **10**, 2302444.

[56] W. Xing, Y. Chen, P. M. Odenthal, X. Zhang, W. Yuan, T. Su, Q. Song, T. Wang, J. Zhong, S. Jia, X. C. Xie, Y. Li, W. Han, *2D Mater.* 2017, **4**, 024009.

[57] N. Wang, H. Tang, M. Shi, H. Zhang, W. Zhuo, D. Liu, F. Meng, L. Ma, J. Ying, L. Zou, Z. Sun, X. Chen, *J. Am. Chem. Soc.* 2019, **141**, 17166.

[58] M.-G. Han, J. A. Garlow, Y. Liu, H. Zhang, J. Li, D. DiMarzio, M. W. Knight, C. Petrovic, D. Jariwala, Y. Zhu, *Nano Lett.* 2019, **19**, 7859.

[59] Z.-W. Lu, S.-B. Qiu, W.-Q. Xie, X.-B. Yang, Y.-J. Zhao, *J. Appl. Phys.* 2020, **127**, 033903.

[60] L. Sun, Y.-X. Zhou, X.-D. Wang, Y.-H. Chen, V. L. Deringer, R. Mazzarello, W. Zhang, *npj Comput. Mater.* 2021, **7**, 1.

[61] M. Agati, M. Vallet, S. Joulié, D. Benoit, A. Claverie, *J. Mater. Chem. C* 2019, **7**, 8720.

[62] A. Redaelli, E. Petroni, R. Annunziata, *Mater. Sci. Semicond. Process.* 2022, **137**, 106184.

[63] X. Zhou, L. Wu, Z. Song, F. Rao, M. Zhu, C. Peng, D. Yao, S. Song, B. Liu, S. Feng, *Appl. Phys. Lett.* 2012, **101**, 142104

[64] W. Zhou, L. Wu, X. Zhou, F. Rao, Z. Song, D. Yao, W. Yin, S. Song, B. Liu, B. Qian, S. Feng, *Appl. Phys. Lett.* 2014, **105**, 243113

[65] X. Zhou, M. Xia, F. Rao, L. Wu, X. Li, Z. Song, S. Feng, H. Sun, *ACS Appl. Mater. Interfaces* 2014, **6**, 14207.

[66] Y. Cheng, D. Cai, Y. Zheng, S. Yan, L. Wu, C. Li, W. Song, T. Xin, S. Lv, R. Huang, H. Lv, Z. Song, S. Feng, *ACS Appl. Mater. Interfaces* 2020, **12**, 23051.

[67] N. M. Ahmed, F. A. Sabah, H. I. Abdulgafour, A. Alsdig, A. Sulieman, M. Alkhoaryef, *Results Phys.* 2019, **13**, 102159.

[68] H. Kim, J. S. Horwitz, G. Kushto, A. Piqué, Z. H. Kafafi, C. M. Gilmore, D. B. Chrisey, *J. Appl. Phys.* 2000, **88**, 6021.

[69] A. H. Ali, Z. Hassan, A. Shuhaimi, *Appl. Surf. Sci.* 2018, **443**, 544.

[70] A. M. Abd-Elhameem, A. Hakamy, *J. Mater. Sci. Mater. Electron.* 2022, **33**, 23293.

[71] F. Ghamari, D. Raoufi, J. Arjomandi, *Mater. Chem. Phys.* 2021, **260**, 124051.

[72] S. Seong, Y. C. Jung, T. Lee, I.-S. Park, J. Ahn, *Mater. Sci. Semicond. Process.* 2018, **79**, 14.

[73] S. Sethuraman, R. A. Gerhardt, *AIP Adv.* 2021, **11**, 105117.

[74] P. K. Song, H. Akao, M. Kamei, Y. Shigesato, I. Yasui, *Jpn. J. Appl. Phys.* 1999, **38**, 5224.

[75] C. G. Granqvist, A. Hultåker, *Thin Solid Films* 2002, **411**, 1.

[76] R. Hamerly, H. Mabuchi, *Phys. Rev. A* 2015, **92**, 023819.

[77] H. S. Sehmi, W. Langbein, E. A. Muljarov, *Phys. Rev. B* 2017, **95**, 115444.

[78] M. W. Song, D. Wang, Z. A. Kudyshev, Y. Xuan, Z. X. Wang, A. Boltasseva, V. M. Shalaev, A. V. Kildishev, *Laser Photonics Rev.* 2021, **15**, 202000343.

[79] L. H, *Color Theory and Modeling for Computer Graphics, Visualization, and Multimedia Applications*, 1997, Springer.

[80] X. Bai, Z. Yang, Z. Xu, Y. Cun, Y. Zi, H. Zhao, Y. Song, Y. He, A. A. Haider, J. Qiu, Z. Song, A. Huang, C. Tatiana, Z. Yang, *Sci. China Mater.* 2023, **66**, 2408.

[81] M. R. Luo, G. Cui, B. Rigg, *Color Res. Appl.* 2001, **26**, 340.

[82] R. Ghinea, M. M. Pérez, L. J. Herrera, M. J. Rivas, A. Yebra, R. D. Paravina, *J. Dent.* 2010, **38**, e57.